First Experimental Demonstration of Full-Duplex Optical Communication on a Single Beam

by

Christopher Garrett and Dr. Thomas Shay

NMSU-ECE-01-009

NMSU-ECE-01-009

First Experimental Demonstration of Full-Duplex Optical Communication on a Single Beam

Christopher Garrett and Dr. Thomas Shay

Manuel Lujan Space Tele-Engineering Program
New Mexico State University
Las Cruces, NM

Prepared for

NASA Goddard Space Flight Center
Greenbelt, MD

under Grant NAG5-9323

May 2001

Klipsch School of Electrical and Computer Engineering
New Mexico State University
Box 30001, MSC 3-O
Las Cruces, NM 88003-8001

FIRST EXPERIMENTAL DEMONSTRATION OF FULL-DUPLEX OPTICAL COMMUNICATION ON A SINGLE BEAM

BY

CHRISTOPHER DAVID GARRETT

A Thesis submitted to the Graduate School in partial fulfillment of the requirements

for the Degree

Master of Science

Major Subject: Electrical Engineering

Minor Subject: Optical Communications

New Mexico State University

Las Cruces, New Mexico

May 2001

"First Experimental Demonstration of Full-Duplex Optical Communication on a Single Beam," a thesis prepared by Christopher David Garrett in partial fulfillment of the requirements for the degree, Master of Science, has been approved and accepted by the following:

Dr. Timothy J. Pettibone
Dean of the Graduate School

Dr. Michael K. Giles
Chair of the Examining Committee

Date

Committee in charge:

Dr. Michael K. Giles, Chair

Dr. Stephen Horan

Dr. Thomas M. Shay

Dr. Z. Charles Ying

ACKNOWLEDGEMENT

I would like to express my appreciation to my advisor, Dr. Thomas M. Shay for all of his help in seeking this advanced degree. His knowledge and wisdom at strange times of day has been an invaluable asset to my studies.

I would also like to thank my spouse, Jasmine, for all of her support. I will pay you back for all of the "child care overtime" that I owe you.

I would also like to thank Dr. Giles for chairing my committee. I put you on the spot and you came through for me on more than one occasion.

A hearty thanks to the members of my committee for agreeing to get me out of here.

Many thanks to NASA Goddard Space Flight Center for their continuing support and funding of the LOWCAL project (grant #xxxx).

Lastly, I thank the other members of the LOWCAL project that have assisted in the measurement, design, and testing of the laboratory experiment. John, Gyungil, and Jason you are greatly appreciated.

CHRISTOPHER DAVID GARRETT

April 2001

VITA

April 19, 1972	Born in Good Samaritan Hospital, Phoenix, AZ
December, 1999	B.S. in Electrical Engineering, New Mexico State University, Las Cruces, NM. GPA=3.95
2000-2001	Klipsch School of Electrical and Computer Engineering, New Mexico State University, Las Cruces, NM.

PROFESSIONAL AND HONOR SOCIETIES

Directed Energy Professional Society

Eta Kappa Nu Electrical Engineering Honor Society

PUBLICATIONS

1. "Lightweight Optical Wavelength Communications without A Laser in space," with D. A. Hazzard, J. MacCannell, G. Lee, J. A. Payne, N. Dahlstrom, and T. M. Shay, Proceedings of the 14th Annual AIAA/Utah State University Small Satellite Conference, 2000.

2. "A Passive Diode Laser Optical Communications Down-link between the Space Shuttle and the Earth," with D. A. Hazzard, J. MacCannell, G. Lee, J. A. Payne, N. Dahlstrom, M. Giles, and T. M. Shay, Proceedings of the International Conference on the Applications of Photonics Technology 2000.

3. "Lightwire a Full-Duplex Optical Communications Link between Earth and the Space Shuttle," with D. A. Hazzard, J. MacCannell, G. Lee, J. A. Payne, N. Dahlstrom, M. Giles and T. M. Shay, Proceedings of the International Conference on the Applications of Photonics Technology 2000.

4. "Novel low-data rate full-duplex optical communications link between earth and LEO," with D. A. Hazzard, J. MacCannell, E. Selves, G. Lee, D. Moore, J. Payne, N. Dahlstrom, and T. M. Shay, Proceedings of the SPIE OptoSouthwest 2000.

5. "System Model for a Low Data Full Duplex Optical Communications Link between Earth and LEO," with D. A. Hazzard, J. MacCannell, E. Selves, G. Lee, D. Moore, J. Payne, N. Dahlstrom, and T. M. Shay, Proceeding of the 35th Annual International Telemetering Conference.

ABSTRACT

FIRST EXPERIMENTAL DEMONSTRATION OF FULL-DUPLEX OPTICAL COMMUNICATION ON A SINGLE BEAM

BY

CHRISTOPHER DAVID GARRETT

Master of Science in Electrical Engineering

New Mexico State University

Las Cruces, New Mexico, 2001

Dr. Michael K. Giles

The satellite industry is driven by the need to reduce costs. One way they have sought to do this is by reducing the size and weight of the satellite because of the extremely high cost per kilogram incurred launching a payload into orbit. The main difficulty in this approach is the lack of power capacity in a small satellite. One of the largest loads on a satellite's power system is the communications system. This has driven the need for a low-power communications system.

This document examines a novel method of communicating optically with a low-Earth-orbit satellite from the ground without the need for a laser on the payload. The goal is to show the feasibility of such a system as a solution to the small satellite low-powered communications problem. Specifically, that the system described

herein: is capable of ground to low-Earth-orbit communications, has very little space-borne mass, and draws little power from the satellite.

First, the system (hereafter referred to as LOWCAL "Lightweight Optical Wavelength Communication without A Laser in space") will be explained with details of the formats used and the link budgets. Discussions will be presented on the development of some of the system hardware (the laser diode driver, liquid crystal driver, and decision electronics for both the up and down links.) Finally, experimental test results of the entire system operating in a laboratory environment are presented and compared to theory.

The results of the laboratory experiment support the original thesis: retro-modulated optical communications can meet the needs of the small satellite community. The system is capable of 10-kbps communication, has low space-borne mass, and draws little power from the satellite (<100-mW measured for the laboratory experiment, <1.5-W calculated for the Shuttle experiment).

TABLE OF CONTENTS

LIST OF FIGURES

LIST OF TABLES

1. INTRODUCTION

1.1 Problem Statement

Launching a satellite (payload) into Earth orbit is a dominant part of its cost. This cost is so large that reducing the weight and size of a satellite is an excellent way to reduce the overall cost of the payload. This has led to the development of micro-satellites, nano-satellites, and pico-satellites, in order from largest to smallest. The smallest pico-satellites are no bigger than a desktop computer, whereas the average micro-satellite is the size of a big-screen television.

One problem with this cost-cutting approach is the lower power generating potential that goes with these small payloads. A full-size satellite may have many square meters of solar arrays, but a small satellite generally has solar cells only on its body. The small satellite project here at New Mexico State University allows only five watts of power maximum for the communications system [1]. This is much less than the tens of watts used by commercial satellite radios.

Clearly, a low-power method of communication is necessary for these small satellites. Whereas there may be RF solutions, an optical system may offer excellent performance and low power needs.

1.2 Summary

This document explores the possibility of using a retro-modulated optical system to communicate with a low-Earth-orbit (LEO) satellite from the ground. Chapter 2 starts with a general discussion of retro-modulated optical communication and a previous experiment.

Then a new method of making a standard retro-modulated optical system operate in a full-duplex mode is presented in Chapter 3, the function of each subsystem described, and the link equations discussed. The theoretical treatment shows the ground-to-LEO link can be closed with a 200-mW ground transmitter and a 6-in diameter retro-modulator.

Chapter 4 covers the hardware development and testing for several parts of the system, mainly for obtaining experimental results and preparing for an eventual Hitchhiker payload on a Shuttle flight coming up in 2002-2003.

A complete laboratory experiment setup is presented in Chapter 5. The hardware setup, adjustment and testing procedures and results are presented and discussed. The results show the system performed as designed with the exception that the signal to noise ratio of the ground receiver was less than expected.

Chapter 6 concludes the document with a few final remarks and suggestions for future work needing to be done on the development of hardware and improvement of the system design.

2. RETRO-MODULATED OPTICAL COMMUNICATION

2.1 Introduction

A communications technique that offers the potential for a low-powered solution to the small satellite platform is called retro-modulated optical communication. A general block diagram of such a system is shown in Figure 2.1.

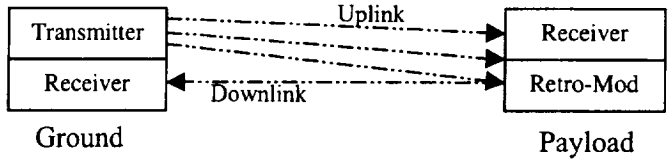

Figure 2.1 Conceptual block diagram of a retro-modulated communication system.

The ground-based transmitter/receiver directs an optical carrier beam to the remote payload. The payload receives any information modulated on the carrier. The payload also retro-modulates (simultaneously retro-reflects and modulates) the carrier back to the ground receiver. The ground receiver then receives and demodulates the returned beam.

The underlying premise of this communications technique eliminates the need for a transmitter on the payload. In traditional optical communication, both ends of the link have a transmitter and a receiver. The traditional layout works well for

terrestrial based systems because pointing, tracking and high transmitter powers are relatively easy to achieve.

However, small satellites do not have the mass required for a precision pointing and tracking apparatus. Nor do they have the power required to transmit at power levels high enough to negate the need for such apparatus. Retro-modulated systems do not require any pointing or tracking at the payload, since they generally have a field of view of 30° or better. The proper orientation of the satellite is enough to ensure good contact with the retro-modulator. Additionally, retro-modulated systems do not have a 'transmitter' in the standard sense; they passively retro-reflect while actively modulating an incident light beam. The power required to modulate this retro-reflected beam is much less than what it would take to transmit a separate beam. This makes a retro-modulated system very attractive.

2.2 Previous Retro-modulator Experiments

In September 1996, a joint team made up of members from Utah State University, Phillips Laboratories, and the U.S. Air Force built and tested a retro-modulated optical communication system [2]. The platform used was a high-altitude weather balloon at an altitude of 30-km. The experiment took place above Kirtland Air Force Base in Albuquerque, NM.

The USU/PL/USAF team built an array of nine retro-modulators to provide the payload with a 45° field-of-view. Each retro-modulator consisted of two

polarizers, a ferro-electric liquid crystal (FLC) modulator, a spoiling lens, and a corner cube reflector. The retro-modulators were designed to intensity-modulate the reflected light. A photo-detector was also placed on the payload, but the system electronics for the uplink were not finished in time for the balloon flight. The ground transmitter operated at 810-nm with an output power of 5-W. The telescope used was the 1.5-m at Starfire Optical Range. Both the uplink and downlink used intensity modulation (On-Off Keying), so the carrier needed to transmit at DC for the downlink to operate. This system was not designed for full-duplex communication.

The payload did have downlink electronics that had several functions. First, it would modulate a 500-Hz signal on the LCD array for two minutes. Then it sent thirty seconds of 1200-bps serial data containing experiment status and test patterns. Afterward, thirty seconds of square waves at 1, 5, and 10-kHz were modulated. Then two more minutes of 1200-bps experimental status and test patterns were sent. Finally, the modulators were left on to measure the scintillation fluctuations.

This experiment proved the possibility of using retro-modulated optical communication in a ground-to-LEO system, making it a success. However, the USU/PL/USAF team was concerned that the modulator technology lacked enough maturity to transmit much faster than 5-kbps without transmitting at a much higher power level.

There are a few problems with the system designed by the USU/PL/USAF team. First, the system did not have the ability to operate in the daytime. A better system would include the ability to filter out daylight from the returned signal.

Second, the transmitter needed to operate at 5-W output power because of the low effective area of the retro-modulator array and the intensity modulation scheme. Lastly, the lack of full-duplex operation was a major shortcoming. A full-duplex system could increase its communications efficiency with the same speed.

3. LIGHTWEIGHT OPTICAL WAVELENGTH COMMUNICATION WITHOUT A LASER IN SPACE

3.1 Introduction

LOWCAL stands for Lightweight Optical Wavelength Communication without A Laser in space. It falls into the category of retro-modulated optical communication. There are a couple of similarities between LOWCAL and the system tested by USU et al. They include: the use of a tracking telescope for collecting the returned signal and a liquid-crystal-based retro-modulator. However, LOWCAL utilizes a novel communications format enabling full-duplex operation and background-rejection filter technology to offer superior performance and the flexibility to operate in the daytime.

The following discussion covers the basics of the LOWCAL system. Detailed discussions of the various segments are in the next chapter. Since the actual communications hardware (i.e. bit synchronization) is not designed yet, the details of data initialization, synchronization, clock recovery, timing jitter, etc. are beyond the scope of this document.

3.2 LOWCAL Transmitter

LOWCAL utilizes a narrow line-width diode laser as the source of optical energy. The wavelength chosen for the experiment is 852.2-nm, due to the optical

properties of the background rejection filter (FADOF) and the availability of a high quality laser diode. A diagram of the transmitter is shown in Figure 3.1. Laser light

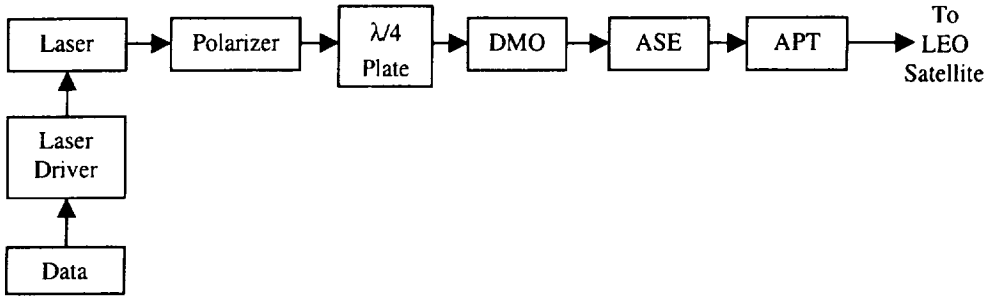

Figure 3.1 LOWCAL transmitter block diagram.

propagates from the source through a crystal polarizer, a quarter-wave plate, the beam divergence management optic (DMO), and finally through the aperture sharing element (ASE) and telescope (APT stands for Advanced Pointer and Tracker, the beam director at White Sands Missile Range) to the satellite.

The data block consists of a computer, micro-controller, or other data source. Binary information flows from the data block into the laser driver, where it is converted into an SC-FSK laser drive current. The laser emits monochromatic light at 852.2-nm into the polarizer. The beam from the laser is only 95% linearly polarized, so the polarizer ensures that a good quality (99.9999%) linearly polarized beam is incident on the quarter-wave plate. The quarter-wave plate converts the linearly polarized light from the polarizer into circularly polarized light. The divergence management optic is computer controlled to adjust the divergence of the optical beam between the acquisition and communication modes. Finally, the

telescope expands and directs the beam to the low-Earth-orbit (LEO) payload/satellite.

The system has two fundamental modes of operation: acquisition mode and communication mode. During the acquisition mode, the divergence of the transmitted beam is set at 0.42-mrad. This will allow the tracking telescope to find and lock onto the target satellite (details of this are in Section 3.7.1). Increasing the integration time of the tracking camera to a few milliseconds is sufficient to acquire the target. The preceding parameters require a down-track uncertainty of 100-m. White Sands Missile Range personnel will provide and operate the satellite-tracking telescope at no cost.

Once the APT system has locked onto the target and stabilized, the divergence management optic will reduce the divergence of the transmitted beam to 20-μrad. The divergence management optic is controlled by a computer connected to a precision motorized translation stage (z-axis only). The time required for the divergence change is about ten seconds.

Uplink data is modulated onto the transmitted beam in the form of sub-carrier frequency shift keying (SC-FSK). If the input data is a logical '0', then an 8.8-MHz tone is modulated onto the circularly polarized transmitted beam. Conversely, if the data is a logical '1', a 10.1-MHz tone is substituted for the 8.8-MHz tone. The frequencies of the tones ensure both proper tracking of the demodulator circuit and excess capability for the data rate (up to 100-kbps) [3]. The modulation depth is 10%

of the total transmitted power. For example, if the average power of the transmitter is 200-mW, the FSK signal power is ±20-mW.

Frequency-shift-keying transmission format was chosen to simplify the space receiver. The initial system design called for a sub-carrier binary phase-shift-keying (SC-BPSK). Phase-shift-keying provides slightly better noise performance than FSK, but there was an excess of 10-dB in signal-to-noise at the space receiver, and an FSK receiver was much simpler to implement. An added benefit of FSK is the elimination of any bit uncertainty – a PSK receiver requires the transmission of a training sequence to know which phase state corresponds to a '1' or a '0'.

3.3 LOWCAL Flight Receiver

The flight receiver detects the optical SC-FSK signal, converts it to an electrical signal, de-modulates it, and sends it to the satellite's CPU. A block diagram for the flight receiver is shown in Figure 3.2. Daytime background light from the

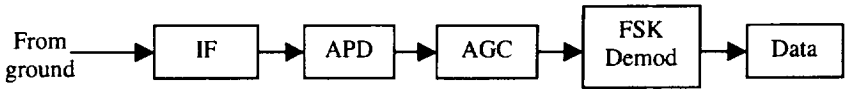

Figure 3.2 LOWCAL flight receiver block diagram.

Earth is reduced to acceptable levels with an optical interference filter (IF). The optical signal power is converted to an electrical voltage by an avalanche photo-diode

module (APD). The signal is then amplified by an auto-gain-control amplifier (AGC). With the signal at the proper amplitude, it is fed into the FSK demodulator.

The FSK demodulator consists of a 74HC4046A CMOS phase-locked-loop (PLL) from Philips Semiconductors. The demodulated output voltage is proportional to the frequency of the input signal. In this case, if the input signal is the 8.8-MHz tone, the output is approximately 1.2 volts. Alternatively, if the input tone is 10.1-MHz, the output goes to around 2.8 volts. The operation of this circuit on a Tektronix TDS-520 sampling oscilloscope is shown in Figure 3.3. Note that the "tones" shown

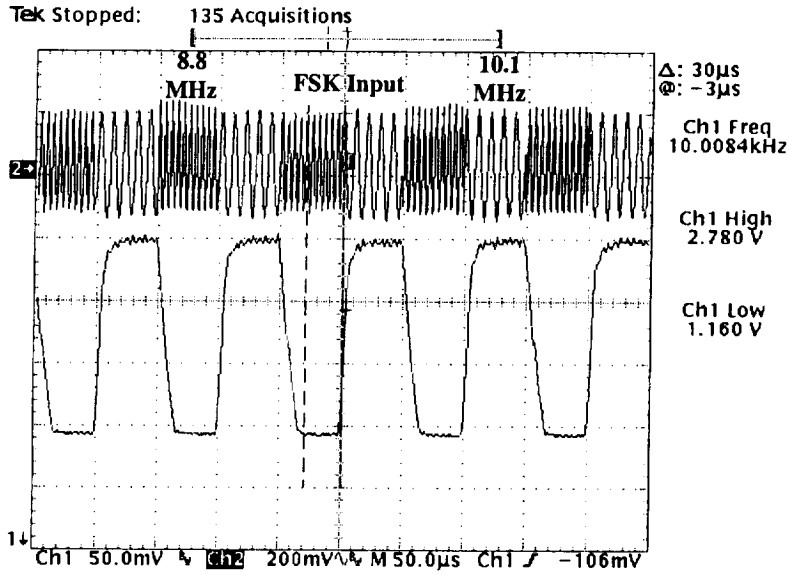

Figure 3.3 FSK demodulation waveform.

in the figure are grossly aliased (the slower tones look faster in the figure due to a sample rate proper for the demodulated signal). Channel 1 is the demodulated output signal shown at 50-mV per division. Channel 2 is the input signal supplied by an

amplified photo-detector module shown at 200-mV per division. The data rate in this example is 20 kbps, and the tones are 10.1 and 8.8-MHz. The SNR of the input signal was around 100, but the demodulated output SNR is more than 300. The FSK tone decoder has high noise immunity due to the use of an exclusive-OR phase comparator in the feedback loop [3].

3.4 LOWCAL Retro-modulator

The retro-modulator allows the satellite to send data back to the ground station. It retro-reflects the circularly polarized carrier back down to the ground receiver where it is collected by the telescope. Circular Polarization Keying (CPK) modulates 100% of the reflected carrier [4]. If the downlink data is a logical '0', then the carrier's polarization is left unchanged. Conversely, if the downlink data is a logical '1', the polarization of the carrier is reversed (i.e. from right-handed circular to left-handed circular). Therefore, the handedness of the returned circular polarization contains the downlink data.

Figure 3.4 shows a block diagram of the retro-modulator. The incident carrier is converted from circular polarization to linear polarization as it passes through the quarter-wave plate. The liquid crystal device (LCD) will then rotate the polarization

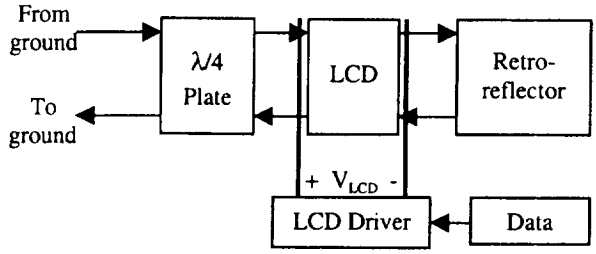

Figure 3.4 LOWCAL retro-modulator block diagram.

either 45° or 0° per pass depending upon the polarity of the voltage across it. Section 4.1 fully treats the design and implementation of the LCD driver hardware and the optimum voltage levels.

3.5 LOWCAL Ground Receiver

Once the retro-modulator modulates the downlink data into the polarization mode of the reflected light, it is collected by the transmitting telescope. A block diagram of the ground receiver is shown in Figure 3.5. After collection, a small

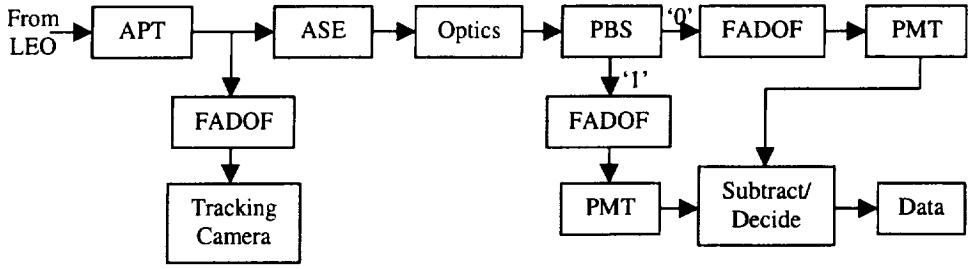

Figure 3.5 LOWCAL ground receiver block diagram.

portion (0.2%) of the returned signal is split off for use by the telescope's active tracking camera. Background radiation is rejected by filtering it with a cesium Faraday Anomalous Dispersion Optical Filter (FADOF), an imaging quality, ultra-high out-of-band rejection optical filter [5], [6], [7], [8]. The FADOF does not degrade the image for the tracking camera and enables the system to operate in the daytime; it rejects up to 60-dB of the solar background radiation [9]. The light that is

not used for tracking is reflected off the aperture-sharing element (ASE), where it is directed to the conditioning optics. The conditioning optics reduce the beam from 10-cm in diameter to about 5-mm in diameter and includes another quarter-wave plate to convert the circular polarization to linear. The linear polarization will depend upon the handedness of the circular polarization and thus the value of the downlink data. A polarization beam splitter (PBS) is then used to discriminate between the two possible polarizations. For example, if the collected light is right-hand circular, the linear polarization is vertical and is propagated straight through the PBS to the '0' leg. If the collected light is left-hand circular, the linear polarization is horizontal and is reflected downward by the PBS to the '1' leg. Each leg filters background light with a FADOF and is then converted to an electrical signal by a high gain photo-multiplier tube (PMT). The signal from each PMT is then subtracted to increase the signal swing and therefore the SNR. A decision circuit is used to determine the downlink data and fed to the ground receiver's CPU.

The subtraction of the PMT signals changes the modulation scheme into Differential Circular Polarization Keying (D-CPK). If the LCD has a zero extinction ratio (meaning the polarization is perfectly right or left-handed), a 6-dB increase in the SNR can be realized over single-ended CPK. Since the extinction ratio (ε) is not exactly zero (3% based on tests detailed in Section 4.1.3), a factor of ($1-2\varepsilon$), will reduce the optimum 6-dB increase. However, the performance is better regardless of

the actual extinction ratio. D-CPK also has the added benefit that a lack of signal is differentiated from one of the bit-states.

3.6 The LightWire Concept

LightWire is the name for a retro-modulated optical communication method that employs the SC-FSK uplink modulation and D-CPK downlink modulation schemes [10]. It was coined by a former student (Jason Payne) when he noticed the full-duplex capability was unique in single-beam optical communication.

If an optical beam is thought of as a channel, just like a coaxial cable or telephone wire, standard optical communication uses a different channel for each direction of a link. However, it is possible to send orthogonal electrical signals down the same channel in different directions at the same time. This is what the LightWire concept says about the LOWCAL system. Data flows in both directions on the same channel (photons in this case).

3.7 LOWCAL Downlink Model

During communication, it is advantageous to have as little beam divergence as possible. Several factors affect the choice of divergence for the transmitted beam. They include atmospheric distortions, coherent speckle, and pointing precision. The atmospheric distortions cause an uncertainty in the directivity (wander) of the optical beam. This translates into an atmospheric-limited beam divergence (θ_{atm}) given by

$$\theta_{atm} \approx \frac{\lambda}{r_0} \tag{3.1}$$

and

$$r_0 \propto \lambda^{7/6} \tag{3.2},$$

where r_0 represents the Fried's parameter and λ represents the wavelength of interest [11]. The Fried's parameter depends not only on the wavelength, but also on the atmospheric conditions. A typical Fried's parameter at 532-nm is 5-cm which corresponds to a Fried's parameter of 8.7-cm at 852-nm. Substituting this value into (3.1) gives an atmospheric-limited beam divergence of

$$\theta_{atm} \approx \frac{852 \times 10^{-9}}{8.7 \times 10^{-2}} = 9.8\text{-}\mu\text{rad} \tag{3.3}.$$

Therefore, a transmit divergence of 20-μrad was chosen as very conservative. In order to ensure a single speckle spot diameter of 7-m in space, the transmitted beam diameter was calculated to be 9-cm.

3.7.1 Modes of Operation

According to the Shuttle Flight Dynamics Officer (FIDO), the typical ephemeris uncertainty is 100-m down-track if the position vector is updated 20 minutes prior to the overpass [12]. This uncertainty in position correlates to about 1/6-mrad. This is more than ten times the divergence of the transmit beam. While it is possible to mechanically scan the telescope, a simpler solution is to increase the

transmitted beam footprint in space to facilitate rapid acquisition. Therefore, the transmitter will operate in two distinct modes: acquisition mode and communications mode.

In the acquisition mode, the beam divergence is increased to 0.42-mrad. This corresponds to a spot diameter of about 260-m in space (at 60° from Zenith). This beam footprint should encompass the retro-modulator, ensure return for the tracking camera, and facilitate rapid convergence of the tracking system. Once tracking is established, the divergence of the transmitted beam will be reduced to the communications mode value (20-μrad).

3.7.2 Received Signal Power

The link budget equation for this system is given by

$$\text{Margin} = P_{TX} - P_{min} - L \qquad (3.4),$$

where P_{TX} is the transmitted power, P_{min} is the minimum required received power needed to communicate at a required BER, and L is the total loss in the link excluding scintillation effects [13]. Since mathematical models of scintillation effects are very immature at optical frequencies, previous experiments offer the best source of data. A margin of 10-dB provided a BER of 10^{-3} to 10^{-4} in the GOLD experiment, which was similar in scale to LOWCAL [14]. Therefore, a margin greater than 10-dB is required for this system to attain a BER of 10^{-6}.

The individual losses are comprised of the modulator efficiency loss (L_{mod}), the atmospheric transmission loss (L_{atm}), the loss due to the telescope and other system optics (L_{opt}), the FADOF transmission loss (L_{FADOF}) and the intercept efficiency loss (L_{SIE}). The sum of the losses excluding L_{SIE} is about 9.5-dB. The signal intercept efficiency loss is given by

$$L_{SIE} = -10\log\left(\frac{A}{R^2 \cdot \Delta\Omega}\right) \qquad (3.5),$$

Where A is the receiver area, R is the one-way propagation length (between 300 and 600-km for a typical LEO [12]), and $\Delta\Omega$ is the solid angle subtended by the transmitted beam. The equation that governs R is given by

$$R = \frac{h_{orbit}}{\cos(\phi)} \qquad (3.6),$$

where h_{orbit} is the altitude of the orbit (320-km is average for the Shuttle and used throughout the calculations) and ϕ is the Zenith angle of the satellite.

The solid angles of the transmitted beam are $\Delta\Omega_{aq}=5.6\times10^{-7}$-sr and $\Delta\Omega_{com}=4\pi\times10^{-10}$-sr for the acquisition and communication modes, respectively. It is assumed that the divergence of the reflected beam and therefore its solid angle will be given by the diffraction of the retro-modulator. Assuming that the satellite is rotated (around the orbital axis) such that one axis is always perpendicular to the transmitted beam, the effective aperture can be modeled as an ellipse dependent upon the Zenith

angle. The optimum angle for a standard 28° Shuttle orbit is α=34° North. The effective area (A_{eff}) of the retro-modulator as seen by the ground is given by

$$A_{eff} = \pi\left(\frac{D_{retro}}{4}\right)^2 \cos(\phi - \alpha) \qquad (3.7),$$

where D_{retro} is the Clear Aperture diameter of the retro-modulator.

The diffraction limited return beam divergence is different for the down-track and out-of-track angles due to its elliptical shape. The diffraction-limited divergence for the down-track angle ($\theta_{ret\,\parallel}$) is given by

$$\theta_{ret\,\parallel} = 0.61\frac{\lambda}{D_{retro}} \qquad (3.8).$$

Similarly, the diffraction-limited divergence for the out-of-track angle ($\theta_{ret\,\perp}$) is

$$\theta_{ret\,\perp} = 0.61\frac{\lambda}{D_{retro}\cos(\phi - \alpha)} \qquad (3.9).$$

Therefore, the diffraction-limited solid angle of the return beam utilizing the small angle approximation is given by

$$\Delta\Omega_{ret} = \pi \cdot \theta_{ret\,\parallel} \cdot \theta_{ret\,\perp} \qquad (3.10).$$

Substituting (3.8) and (3.9) into (3.10) results in the final solid angle of the return beam,

$$\Delta\Omega_{ret} = \frac{\pi}{\cos(\phi - \alpha)}\left(\frac{0.61 \cdot \lambda}{D_{retro}}\right)^2 \qquad (3.11).$$

Now an equation can be written to express the power received at the ground. In linear form, the received signal power (P_S) is given by

$$P_s = P_{TX}\frac{(\eta_T \cdot \eta_{mod} \cdot \eta_{atm})^2 \eta_{retro} \cdot \eta_{RBT} \cdot T_{FADOF} \cdot A_{eff} \cdot A_r}{R^4 \cdot \Delta\Omega_{tip} \cdot \Delta\Omega_{ret}} \qquad (3.12),$$

where η_T, η_{mod}, η_{atm}, η_{retro}, and η_{RBT} are the single-pass transmissions of the telescope, LCD modulator, atmosphere, retro-reflector, and receiver beam-train, respectively. T_{FADOF} is the signal transmission of the FADOF, and A_r is the area of the telescope's Clear Aperture. Substituting (3.6), (3.7), (3.11), and the transmit beam solid angle into (3.11) yields

$$P_S = P_{TX}(\eta_T \cdot \eta_{mod} \cdot \eta_{atm})^2 \eta_{retro} \cdot \eta_{RBT} \cdot T_{FADOF} \cdot \frac{A_r \cdot D_{retro}^4 \cdot \cos^4(\phi) \cdot \cos^2(\phi - \alpha)}{h_{orbit}^4 \cdot \pi(1.22\lambda)^2 \cdot \theta_{TX}^2} \qquad (3.13).$$

The received signal power depends upon the fourth power of both the orbital altitude and retro-modulator diameter. However, it depends upon the sixth power of the cosine of the Zenith angle. Therefore, a small decrease in the acquisition intercept angle of the satellite will greatly reduce the required transmitter power. A graph of this relationship for both an overhead orbit and a typical 28° Shuttle orbit (α=34°) is

shown in Figure 3.6. The maximum received power occurs at the Zenith angle closest to zero and falls off rapidly. For the 28° Shuttle orbit, the received power at a 60° Zenith angle is fifteen times less than maximum. The ground receiver is designed to handle this variation.

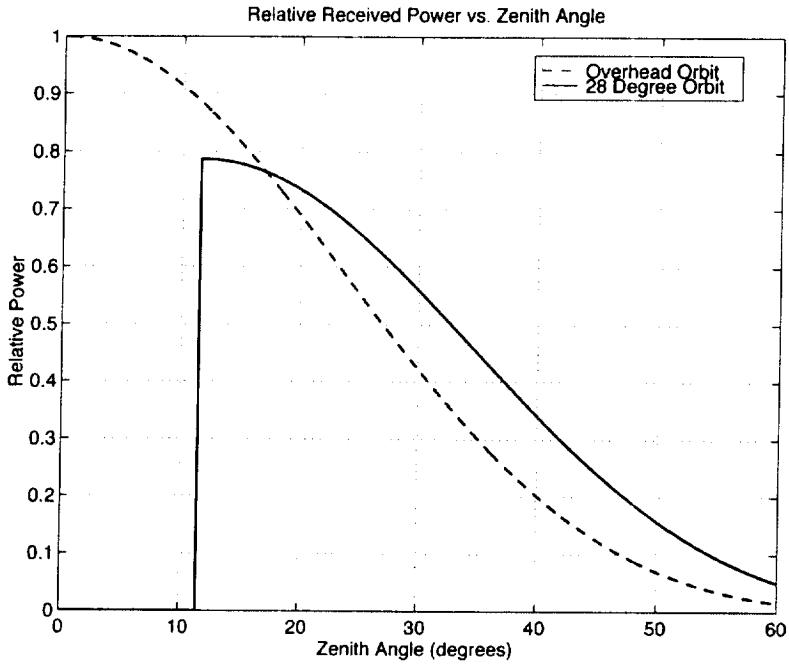

Figure 3.6 Relative received signal power vs. Zenith angle for two orbits.

Table 3.1 System Parameters

Parameter	Value
Transmitter Power	−7-dB (200-mW)
Receiver Diameter	60-cm
Retro-modulator Diameter	6-in

Data Rate	10-kbps
Acquisition Integration Time	0.01-sec
Scintillation Margin	10-dB
Atmosphere Loss	3-dB
LCD Modulator Loss	1.4-dB

Table 3.1 – *Continued*

Parameter	Value
Telescope loss	0.36-dB
Receiver beam train loss	0.9-dB
FADOF Loss	1-dB
Retro-reflector Loss	0.25-dB
Transmit Beam Divergence (Communications)	20-μrad
Transmit Beam Divergence (Acquisition)	420-μrad
Acquisition Intercept Angle	60°

Given the link parameters listed in Table 3.1, the total round-trip signal intercept efficiency loss at the acquisition intercept angle are 80 and 104-dB for the communications mode and acquisition mode, respectively. The 24-dB difference between them is due solely to the difference in the divergence of the transmit beam.

The received optical signal power is given by

$$P_S = P_{TX,dB} - L_{TOTAL} \qquad (3.14),$$

where

$$L_{TOTAL} = 2(L_T + L_{mod} + L_{atm}) + L_{retro} + L_{RBT} + L_{FADOF} + L_{SIE} \qquad (3.15).$$

Therefore, substituting the parameters from Table 3.1 into (3.14) and (3.15) yield expected signal powers of 2.2-nW and 8-pW for the communications and acquisition modes, respectively. Of course, the scintillation effects were not included in the above powers, so the required SNR of the ground receiver must be at least 10-dB lower than a signal level of 2.2-nW provides.

3.7.3 Signal to Noise Ratio

Assuming D-CPK communications and negligible inter-symbol interference, the downlink SNR is given by

$$\mathrm{SNR} = \frac{\left(2 \cdot P_S \cdot G \cdot (1-2\varepsilon) \cdot \Re\right)^2}{\left(\begin{array}{c} 2 \cdot q \cdot G^2 \cdot B \cdot P_S \cdot (1-2\varepsilon) \cdot \Re + 2 \cdot q \cdot G^2 \cdot B \cdot P_{sky} \cdot \Re + \\ 2 \cdot q \cdot G \cdot B \cdot I_D + \dfrac{4 \cdot k_b \cdot T \cdot B \cdot F_L}{R_L} \end{array}\right)} \qquad (3.16),$$

where ε is the LCD extinction ratio, $\Re$ is the PMT responsivity in A/W, q is the electron charge, G is the PMT current gain, B is the noise equivalent bandwidth, P_{sky} is the background power that gets through the FADOF, I_D is the dark current at the PMT anode, k_b is Boltzman's constant, T is the temperature of the load resistance in

degrees Kelvin, F_t is the noise figure of the amplifier, and R_L is the load resistance [13]. The denominator of (3.16) is made up of four individual noise terms. The first term is the quantum noise due to the signal (or signal-shot) noise, the second term is the quantum noise due to background power, the third term is the quantum noise of the PMT dark current, and the last term encompasses both the Johnson noise and electronic noise.

The SNR required for a BER of 10^{-6} is 19.6-dB. This assumes unbiased data and a receiver threshold set halfway in between the '1' and '0' levels. The expected signal level of 2.2-nW needs to produce a signal to noise ratio of 29.6-dB in order to have a 10-dB scintillation margin.

The solar noise that gets through the FADOF could be significant, so it shall be analyzed first. The solar noise incident on each PMT is given by

$$P_{sky} = \frac{\partial L_e}{\partial \lambda} \cdot \Omega_{RX} \cdot A_r \cdot \Delta\lambda_{FADOF} \cdot T_{FADOF} \cdot \eta_T \qquad (3.17),$$

where $\frac{\partial L_e}{\partial \lambda}$ is the spectral radiance of the blue sky, Ω_{RX} is the solid angle of the receiver and $\Delta\lambda_{FADOF}$ is the optical bandwidth of the FADOF. The solar spectral radiance of the sky at 1-μm is [15]

$$\frac{\partial L_e}{\partial \lambda} = 10^3 \frac{\mu W}{cm^2 \cdot sr \cdot \mu m} \qquad (3.18).$$

The spectral radiance of the blue sky roughly maintains the value given in (3.18) as long as the detector is pointed more than 10° away from the sun. The total optical bandwidth of the optimum FADOF is 0.002-nm and its transmission is 80%. The solid angle of the receiver is $\Omega_{RX,\,comm}=1.27\times10^{-9}$-sr and $\Omega_{RX,\,aq}=3.6\times10^{-7}$-sr for the daytime communications and acquisition modes, respectively. Substituting (3.18) and the other known quantities into (3.17), the optical power of the sky incident on each PMT is 5-fW and 1.4-pW for the daytime communications and acquisition modes, respectively.

The measured characteristics of the PMT receivers are summarized in Table 3.2 [16]. With the parameters in the table and P_{sky}, it is easily shown that the receiver system is dominated by quantum signal-shot noise. Figure 3.7 shows the SNR limited by each contributor and the total SNR. The SNR is clearly signal-shot limited for received powers above 1-pW.

Table 3.2 PMT receiver characteristics.

Parameter	Value
Quantum efficiency	1.1%
Responsivity at 852-nm	7.89-mA/W
Current gain	520-kA/A
Anode dark current	1.6-nA
Load resistance	100-kΩ

3-dB bandwidth	20-kHz
Noise figure	~1

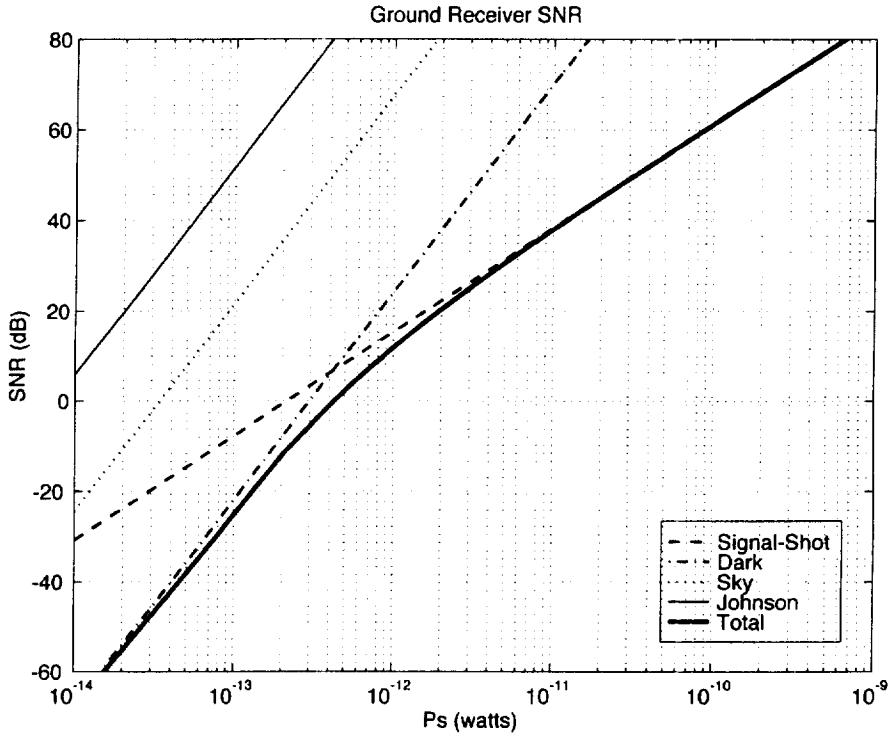

Figure 3.7 SNR of the ground receiver during daytime communications.

Therefore, the SNR reduces to

$$\mathrm{SNR} = \frac{2P_S \cdot (1-2\varepsilon) \cdot \eta_{PMT}}{h\nu \cdot B} \qquad (3.19),$$

where η_{PMT} is the quantum efficiency of the PMT and $h\nu$ is the energy of an 852-nm photon. If (3.19) is re-arranged to find the minimum signal power for a given minimum SNR, the result is

$$P_{S,\,min} = \frac{\mathrm{SNR}_{min} \cdot h\nu \cdot B}{2 \cdot (1-2\varepsilon) \cdot \eta_{PMT}} \qquad (3.20).$$

The minimum signal power is proportional to the minimum SNR, the noise equivalent bandwidth, and inversely proportional to (1-2ε). Substituting known values into (3.20) results in a minimum received signal power of

$$P_{min}=20.5\text{-pW} \qquad (3.21)$$

for a BER of 10^{-6}. If a 10-dB scintillation margin is included, we need to receive 0.21-nW.

For a transmitted power of 200-mW, the calculated signal power is 2.2-nW at a Zenith angle of 60°. If SNR_{comm} refers to the SNR with 2.2-nW of received power, the link margin is given by

$$M = 10\log\left(\frac{\mathrm{SNR}_{comm}}{\mathrm{SNR}_{min}}\right) \qquad (3.22).$$

In the quantum-shot limited case, (3.22) reduces to

$$M = 10\log\left(\frac{P_S}{P_{min}}\right) \tag{3.23}$$

Substituting both (3.21) and the 2.2-nW result into (3.23) yield a margin of 20.3-dB. The overall system margin becomes 10.3-dB after subtracting a 10-dB scintillation margin.

3.8 LOWCAL Uplink Model

As described in Sections 3.3 and 3.4, the uplink consists of the ground transmitter and an FSK receiver on the satellite. The average optical power detected by the satellite's photo receiver is given by

$$P_{ave} = E_{ave} \cdot A_d \tag{3.24}$$

where E_{ave} is the average irradiance at the satellite and A_d is the area of the detector. Assuming the use of an Avalanche Photo Diode (APD), the SNR of the signal into the FSK demodulator is given by

$$SNR = \frac{(m \cdot P_{ave} \cdot M \cdot \Re)^2}{\left(\begin{array}{l} 2 \cdot q \cdot B \cdot P_{ave} \cdot M^2 \cdot F(M) + 2 \cdot q \cdot B \cdot I_L + \\ 2 \cdot q \cdot B \cdot I_{BD} \cdot M^2 \cdot F(M) + \dfrac{4 \cdot k_b \cdot T \cdot B \cdot F_t}{R_L} \end{array}\right)} \tag{3.25}$$

where M is the APD gain, P_{ave} is the average power given by (3.24), m is the modulation index, $F(M)$ is the excess noise factor ($M^{0.7}$ for silicon), B is the noise

equivalent bandwidth (12-MHz), I_L is the surface leakage current, I_{BD} is the bulk dark leakage current, T is the temperature of the load resistance, R_L is the load resistance, and F_t is the noise figure of any additional amplification (from the AGC) [13].

The average irradiance at the satellite is 50-nW/cm^2, assuming the system is operating in communications mode and the transmitter power is 200-mW. The FSK modulation index is 10% (m=0.1). If a silicon Avalanche Photo Diode (APD) module is used at the payload having an area of 4-cm^2, the SNR at the FSK demodulator should be 40-dB. This leaves an uplink margin of 20-dB.

4. SUB-SYSTEM HARDWARE DESIGN AND TESTING

4.1 LCD Driver

The first LCD system purchased for LOWCAL consisted of a DisplayTech LCD with a bench top driver. Unfortunately, the optical rise time of the LCD was too long for 10-kbps communication. We then obtained a phase-separated composite liquid crystal device (LCD) from Dr. Satyendra Kumar at Kent State University that could potentially operate faster than the device purchased from DisplayTech [17]. Kent State University said that it should be driven with a ±10-volt square wave. The circuit model provided with the device was a capacitor with leakage resistance. Table 4.1 lists the design requirements for the LCD driver. The requirements in the table

Table 4.1 LCD driver design requirements.

Parameter	Value
Electrical 3-dB frequency	20-kHz
Drive voltage capability	±5 to ±12-V
High-Z output state?	YES
Scalable?	YES
Input signal levels	TTL
Minimum power efficiency	80%

reflect the need for the system to be both versatile and low-powered. A more detailed account of Section 4.1 can be found in [18].

4.1.1 Design Process

Before designing a circuit, it was important to characterize the LCD in terms of an electrical load. The device was connected to an RLC meter and the following measurements were made: 35-nF shunt capacitance and 1-MΩ shunt resistance. These values for the resistance and capacitance of the LCD gave it a natural cutoff frequency of 4.5-Hz. In order to meet the required 3-dB frequency, the driver needed to have an output resistance of less than 200-Ω. It was also determined that a driver with lower output impedance would have a higher power efficiency. The adjustable drive voltage level was required to characterize the optical performance (speed) of the LCD as a function of the drive voltage.

Several circuits were suggested before a good solution was found. The initial designs worked well, but they dissipated too much power (50 to 70% efficiency) and took several cycles of the signal to stabilize. The final design was both simple and rugged, while dissipating almost no quiescent power and very little dynamic power. It is comprised of a pair of complimentary SPST CMOS analog switches (MAXIM model number MAX303) to alternately connect the load directly to a pair of adjustable power rails. An additional CMOS switch (MAXIM model number MAX4590) connects the output to the LCD. The total output resistance of the driver

is 15Ω (using MAXIM data sheet values for the on-resistance) and provides an electrical 3-dB frequency in excess of 300-kHz. The circuit diagram appears in Figure 4.1.

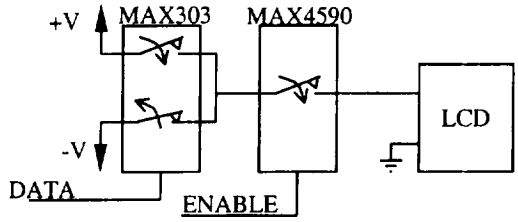

Figure 4.1 LCD driver circuit.

4.1.2 LCD Driver Testing

The driver was tested in the configuration used for the final system design. The output from the driver was connected directly to the LCD supplied by Kent State University. The Tektronix TDS-520 sampling oscilloscope was used to measure the system rise time; results are shown in Figure 4.2. The measured rise time is about 800-ns, this is 30% better than expected and corresponds to an output resistance of 10.4-Ω and a 3-dB bandwidth of 440-kHz (ten times better than required).

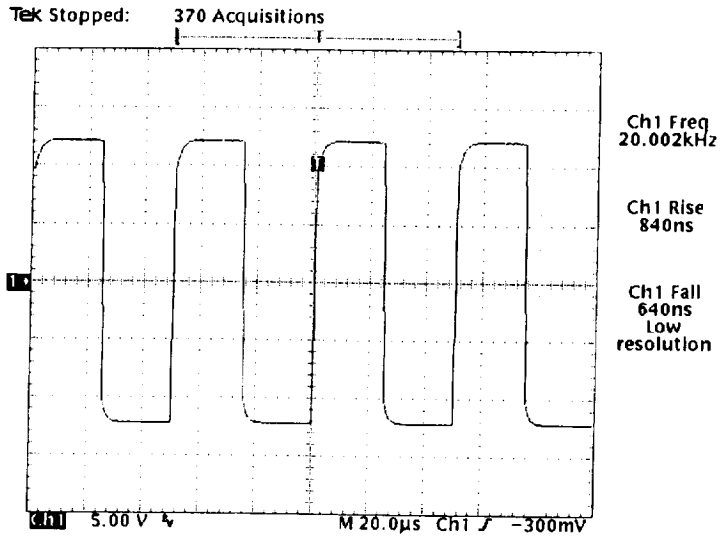

Figure 4.2 LCD drive waveform with rise and fall time measurements.

4.1.3 LCD Optical Performance Testing

After measuring the LCD driver's capabilities, the optical performance of the LCD needed to be characterized. The main purpose of this test was to find a level of drive voltage that balanced the optical performance with the LCD power consumption. Knowing the LCD was mainly a capacitive load, the power consumption was dominated by dynamic (switching) power given by

$$P_{dyn} = 2f \cdot C_L \cdot V_+^2 \qquad (4.1),$$

where f is the modulation frequency, C_L is the capacitance of the LCD, and V_+ is the voltage of the positive rail of the bi-polar system. Since the power dissipated in the LCD is proportional to the square of the drive voltage, finding the minimum voltage that gave good performance (2% extinction ratio at 20-kbps) was the goal.

Figure 4.3 shows a layout of the optical test done on the LCD. The polarizers

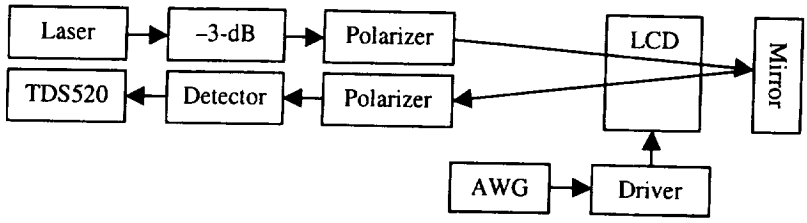

Figure 4.3 Test layout for optical characterization of the LCD.

were adjusted for intensity modulation of the LCD (the polarizers were crossed by 90°). The polarizers were further tuned to give maximal contrast between the on and off states of the system at a 10-Hz drive frequency (close enough to DC that the LCD would fully rotate). Data was collected at drive levels of ±8-V, ±10-V, and ±12-V. The modulation frequency was varied from 1-kHz up to 50-kHz at 1-kHz intervals. Figure 4.4 shows a graph of the results from zero to 10-kHz. The assumed operation frequency was 10-kHz, and the maximum desired extinction ratio was 2%. It is clear from the figure that a drive level of ±12-V offers performance that is superior to the other two test cases. The target extinction ratio of 2% was not met, but a higher level of drive was considered too costly in terms of the power dissipation. Therefore, the ±12-V drive level was chosen as optimal.

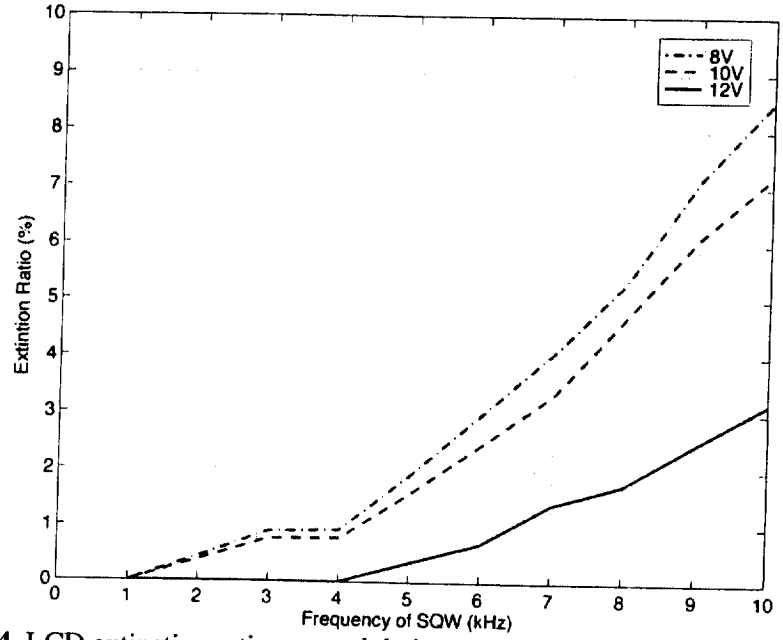

Figure 4.4 LCD extinction ratio vs. modulation rate at three levels of drive.

4.1.4 LCD Power Consumption Measurement

With a chosen modulation frequency and drive level, the actual power consumption of the LCD needed to be measured. Substituting f=10-kHz, V_+=12-V, and C_L=35-nF into (4.1), the power dissipation was predicted to be 100-mW. Figure 4.5 shows the electrical connections made to measure the instantaneous power dissipation in the LCD. The differential amplifier is a Stanford Research Systems model SR560. It was set to a gain of 1, and the offset was trimmed to zero just before the measurement. The TDS-520 sampling oscilloscope was set to multiply channels 1 and 2 together and display the resulting waveform. The average value of the resulting waveform was also calculated by the oscilloscope. Figure 4.6 depicts the results, which are consistent with the 100-mW expected. The average power

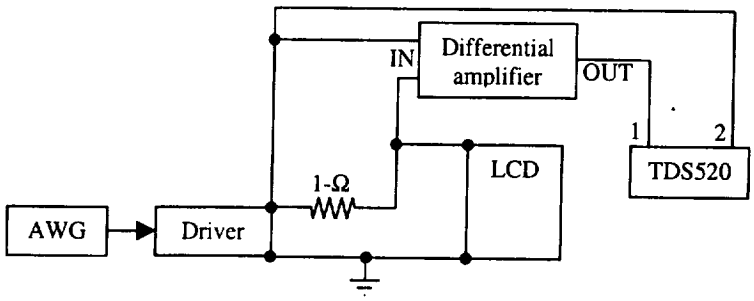

Figure 4.5 LCD power consumption test setup.

consumption was measured as 93-mW. The peak power consumption occurs during the charging of the LCD capacitance and has a value of 1.6 watts.

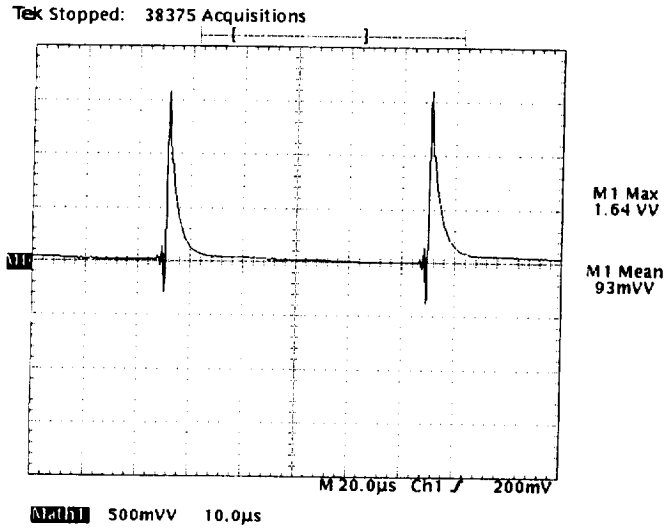

Figure 4.6 Instantaneous power dissipated by the LCD at ±12-V and 10-kHz.

The power dissipated in the driver is composed of two components, the dynamic dissipation due to charge injection and the resistive dissipation due to the output resistance of the driver. The resistive power is given by

$$P_R = \left(\frac{P_{rms}}{V_{rms}} \right)^2 R_{out} \qquad (4.2),$$

where P_{rms} and V_{rms} are the measured quantities, and R_{out} is the worst case output resistance (15-Ω). Substituting measured values into (4.2) results in a resistive power dissipation of 0.9-mW. The power dissipated by the charge injection is given for the ±12-V switch circuit as

$$P_{DD} = f \cdot Q \cdot V_+ \qquad (4.3),$$

where Q is the charge injection for the analog switch. The power dissipated in the first switching network (the bi-polar driver) comes out to 1.2-μW, and the second switch (the output enable) can be ignored since it is not switched at a constant rate. Therefore, the total power dissipated by the LCD driver is 0.9-mW. The power efficiency of the driver circuit is therefore calculated as 99%. The high power efficiency of the LCD driver allows for any necessary DC-DC voltage conversion to have as poor as 81% efficiency and still maintain an overall efficiency of 80%; this is important because satellites often have high voltage (~30-V) power systems.

4.2 Laser Driver

The two laser diodes purchased for the LOWCAL experiment were μLs Lepton II laser modules. These modules contain a Spectra Diode Labs 852.2-nm Distributed Feedback (DFB) laser diode, output optics that circularize and collimate

the beam, a thermistor, and a thermo-electric cooler (TEC) in a compact package. Temperature controllers were also purchased from μLs, as well as a pair of high-speed drivers (model number DB-MHZ-500) for the laser diodes. Unfortunately, drivers available from commercial sources are all designed for on-off keying and possess limited DC drive capability. The drivers purchased with the laser modules were no exception and deemed unsuitable for the task, making it necessary to design custom drivers. A more detailed account of Section 4.2 can be found in [19].

4.2.1 Design Process

Table 4.2 summarizes the design requirements for the laser driver. The task was to design, build, and test a circuit that could meet these requirements. After designing two different circuits and building them into oscillators, the commercial drivers were re-examined.

Table 4.2 Design requirements for the laser driver.

Parameter	Value
DC drive current	0 to 200-mA
AC drive current	0 to 50-mA
3-dB signal bandwidth	15-MHz
FSK tone generation	8.8 & 10.1-MHz
Data input signal levels	TTL
Maximum data rate	50-kbps

Gentle power-up	YES

Table 4.3 Properties of μLs DB-MHZ-500 driver.

Parameter	Value
DC drive current	0 to 40-mA
AC drive current	0 to 200-mA
3-dB signal bandwidth	500-MHz
Data input signal levels	ECL
Gentle power-up	YES

Table 4.3 summarizes the capabilities of the drivers purchased from μLs. The DB-MHZ was clearly unsuitable if used alone, but could be used if the output from two could be combined. Combining the output from two of these drivers was deemed possible due to the way in which they operate. These particular devises act like controlled current sinks. They actually pull current through the laser diode and have a common ground at the shield of the drive cable.

The output from both drivers was combined through a MiniCircuits RF Bias-Tee (model number ZFBT-6GW). One driver was used to supply all of the DC current by setting the data input to '1'. The other driver supplied the entire AC signal current. A simplified circuit diagram is shown in Figure 4.7. The figure also shows a control/readout block that controls the current of each driver and displays the output on a digital readout.

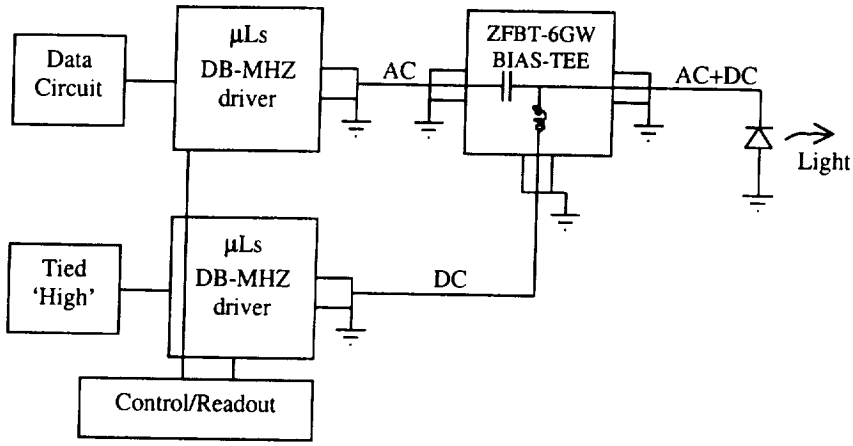

Figure 4.7 Simplified circuit diagram showing two commercial drivers driving the same laser diode.

Now that the current source was complete, a tone generator was needed to convert TTL binary data into the specified 8.8 and 10.1-MHz tones. This was done with a Hewlett Packard Arbitrary Waveform Generator (AWG), model number 33120A. The settings for the AWG are shown in Table 4.4.

The output from the AWG is an analog FSK data signal, but it is not in a format that the laser driver understands, therefore the signal must be transformed into ECL logic. This was done by feeding the output of the AWG into a voltage comparator. The output from the voltage comparator is fed into a TTL-ECL converter IC (Motorola part# MC10H424P). The output from the TTL-ECL converter is then cabled to the DB-MHZ-500 driver. A block diagram of the circuit is shown in Figure 4.8, and a photo of the completed hardware is in Figure 4.9.

Table 4.4 Arbitrary waveform generator settings.

Parameter	Value
Signal type	SINE
Amplitude	2.0-VPP
DC offset	+130-mV
Frequency	8.8-MHz
Modulation	FSK
FSK frequency	10.1-MHz
FSK source	EXT

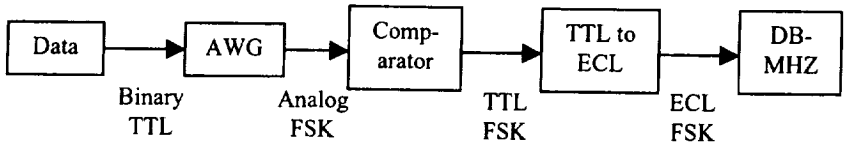

Figure 4.8 Process of converting TTL data into ECL FSK.

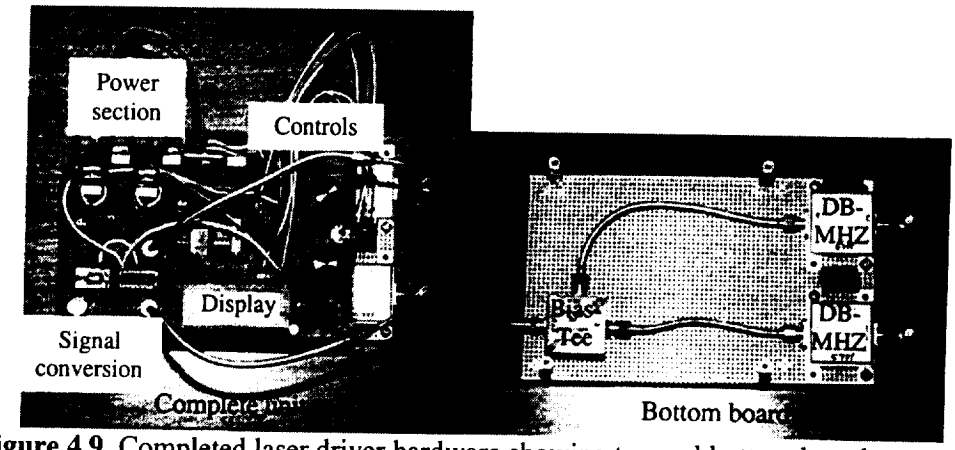

Figure 4.9 Completed laser driver hardware showing top and bottom boards.

The power supply, controls and display circuitry were made as specified in the DB-MHZ-500 user's manual. Each DB-MHZ-500 got its own regulator for –12-V and –5.2-V. The TTL to ECL converter shares a –5.2-V regulator with the DB-MHZ-500 that supplies the AC signal. The comparator and TTL to ECL converter chips also needed +5-V. A large ±15-V power supply was used as the input to all on-board regulators.

The readout circuitry for one of the DB-MHZ-500's consists of an OPA-27 op-amp configured as a differential amplifier, with a voltage divider on the output. The output current from the DB-MHZ-500 is the voltage between two of its pins divided by 2.5. The simple analog circuit created a voltage directly proportional to the drive current. This voltage was wired to the input of the LCD panel meter. Once adjusted, the circuit maintained an error of less than 1-mA, which is acceptable for this application. A circuit diagram for a single readout circuit is shown in Figure 4.10. Both drivers have a dedicated readout circuit to eliminate the possibility that the additional load would change the driver's output current.

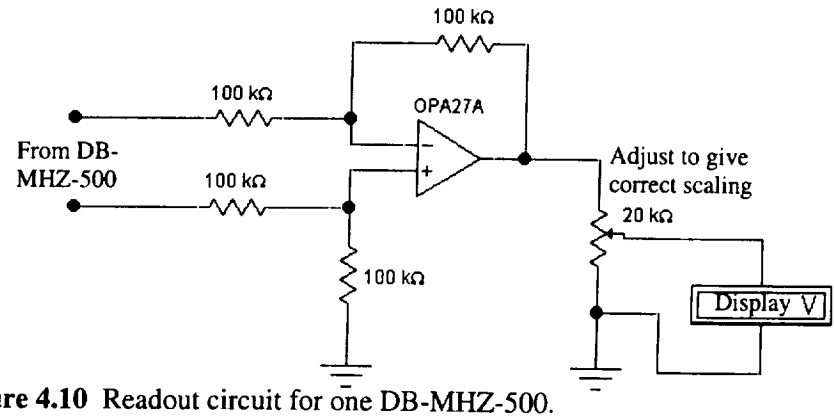

Figure 4.10 Readout circuit for one DB-MHZ-500.

The OPA-27 features low noise, and low offset drift. The input offset was manually trimmed with an additional potentiometer as per the Burr-Brown data sheet. The offset adjustment is simple: short the inputs together and adjust until the output is zero volts. The output pot was adjusted such that a 0.5-V differential across the input terminals gives a voltmeter reading of 0.200-V. This calibration procedure nulls any error in the differential gain of the circuit. Having built a prototype, the system was tested with a low-cost visible (670-nm) diode supplied with the Lepton II.

4.2.2 Hardware Testing

The prototype driver was attached to a test laser diode. The output of a solitary laser diode is highly divergent, so a short focal length lens was placed in front of the diode to roughly collimate the output. A high-speed NewFocus visible photo-detector module (model number 1801) was placed about two feet away from the laser such that the laser light illuminated the detector.

With an oscilloscope attached to the photo-detector output, test tones were generated by the AWG and transmitted at different power levels through the test setup. The amplitude and DC offset of the AWG was determined during this stage to give an optical waveform that was close to 50% duty cycle. Having 50% duty cycle tones is important due to the X-OR phase comparator in the FSK demodulator. The quality of the optical signal was deemed good enough (correct duty-cycle and undistorted) to progress to the next stage of testing.

Having found the driver settings that gave a signal output swing appropriate for the FSK demodulator (400-mV P-P), an FSK test pattern was entered into the AWG. The FSK circuit was previously tested with the AWG connected directly, but now the photo-detector output was cabled to the FSK demodulator. Square wave signals up to 25-kHz were successfully transmitted, received, and demodulated by the test setup.

5. LABORATORY EXPERIMENT

With all of the system components built and tested individually, it was time to test the entire system. Therefore, decision circuits were built to make all data input and outputs TTL compatible, and a digital transmission analyzer was obtained from another laboratory. This chapter presents the experimental setup and results, followed by a discussion of the experimental vs. expected behavior.

5.1 Laboratory Experiment Setup

The laboratory system is broken up into two main parts: the "ground station" and the "payload." The ground station consists of an optical table on which is mounted the transmitter system, the aperture-sharing element, and the ground receiver system. The payload is located on a mobile cart three rooms away (20-m) and consists of the space receiver and the retro-modulator. Pictures of the ground station and payload are shown in Figures 5.1 and 5.2, respectively. A comparison between the LOWCAL system presented in Chapter 3 and the experimental setup is summarized in Table 5.1.

Figure 5.1 The laboratory experiment ground station.

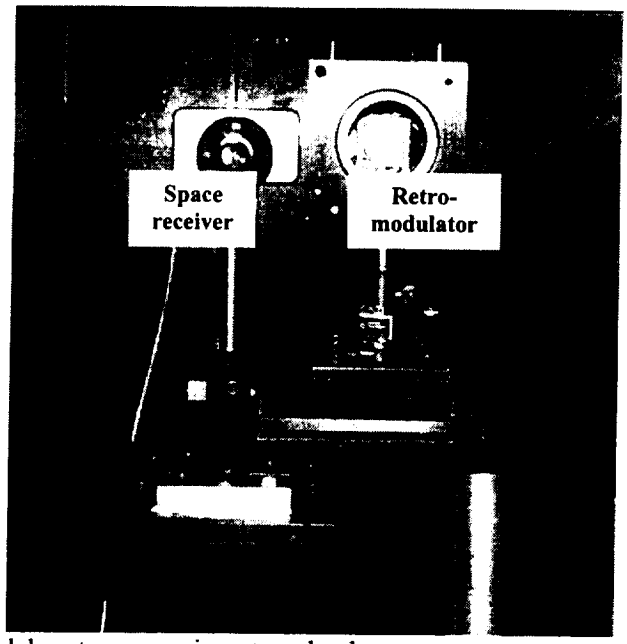

Figure 5.2 The laboratory experiment payload.

Table 5.1 Comparison of LOWCAL to the experimental setup.

Description	LOWCAL	Experiment
Range	320-km	20-m
Transmitter power	200-mW	10-mW
Transmitted beam divergence	20-μrad	100-mrad
Telescope?	YES	NO
Number of lasers	2	1
Number of drivers per laser	2	1
Signal power at payload	18-nW	12-μW
Space optical receiver	APD	PIN
Retro-modulator area	182-cm^2	4-cm^2
Downlink keying	D-CPK	CPK
Number of FADOF/PMT's	2	1
Signal power at ground	2.4-nW	4-nW

5.2 Pre-Experiment Procedures

Before the system could be tested, all of the various subsystems needed measuring, aligning, calibrating, etc. This section will present the various issues and the procedures developed to correct them. A more detailed version of Section 5.2 can be found in [20].

5.2.1 Polarization Quality of the Transmitted Beam

The first detected problem was in the circularity of the transmitted beam. The transmitter's quarter-wave plate was adjusted to the correct position based on finding a crystal axis and then rotating the quarter-wave plate 45°. However, after measuring the transmitted beam, it was discovered to be more than 20% elliptical (one polarization direction contained 20% more power than the other direction).

Clearly, aligning the quarter-wave plate based on the tick-marks on the mount was not good enough to provide a circularly polarized beam. The test setup shown in Figure 5.3 was devised to ensure a good quality transmitted beam. The second

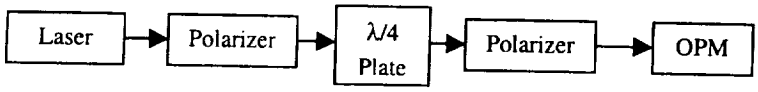

Figure 5.3 Test setup to ensure a circularly polarized transmitted beam.

polarizer is rotated 360° about the optical axis while watching the reading on the optical power meter (OPM). If the power reading stays constant (±1%) then the transmitter is properly adjusted. If the power reading fluctuates, then the quarter-wave plate is rotated slightly, where the power measurement process is repeated. After a few iterations of this procedure, the beam should be of acceptable quality (less

than ±1% variation). Note: the adjustment is very sensitive – the quarter-wave plate is easily rotated through the optimal orientation.

5.2.2 Alignment of the Retro-modulator

Ideally, the fast axis of the retro-modulator's quarter-wave plate should be aligned with the fast axis of the LCD in one drive state. This is important to give good signal quality at the ground receiver. This is accomplished by rotating the payload quarter-wave plate while transmitting a carrier and modulating a slow (100-Hz) test signal onto the LCD.

Adjusting the quarter-wave plate to give a maximum signal swing at the PMT system provides optimal performance. In this position, the average value of the PMT signal will stay constant as the frequency of the test signal is increased. An invariant average signal makes the decision process easier at the ground receiver. This procedure may change once another FADOF/PMT is added to the system and the signal is detected differentially.

5.2.3 Adjustment of the Ground Receiver

The ground receiver also contains a quarter-wave plate that must be properly aligned with the input polarizer of the FADOF. Using the same 100-Hz test signal as in Section 5.2.2, the ground receiver quarter-wave plate must be rotated until the signal swing out of the PMT is maximized.

5.2.4 Signal Transmission Through the FADOF

Every FADOF is slightly different from every other FADOF. This is caused by slight variations in the temperature controlling hardware, thermo-dynamic design of the enclosure, variation in the vapor cell manufacturing, and variation in the magnetic field. Therefore, each FADOF must be characterized in order to optimize performance.

The characterization procedure is comprised of three main steps. First, measure the magnetic field with a calibrated Gauss meter and compare with theoretical calculations to decide on a starting temperature. Second, with the FADOF at the temperature decided on in step one, measure the transmission curve by varying the wavelength of the source, noting the locations, spacing, and FWHM of the transmission peaks. Be sure to record either the wavelength or the laser diode temperature accurately enough to find the transmission peaks later. Third, if the results are unsatisfactory, change the temperature 2°-C up or down and repeat step two. Repeat step three until the desired pass-band shape is attained.

The FADOF used in the laboratory experiment has a magnetic field of about 100-Gauss. The optimum magnetic field for the LEO experiment is 50-Gauss, which causes the central two transmission peaks to combine into one 5-GHz wide peak. The transmission of the laboratory FADOF is shown in Figure 5.4. The wavelength axis was calculated from measuring the voltage across the laser diode's thermistor and applying an empirically derived relationship between the wavelength and that voltage. The thermistor voltage was used because the wavelength-measuring device

in the laboratory lacks the precision required to map the transmission curve with any detail (but it was good enough to measure the relationship between the thermistor voltage and the wavelength). The optimum temperature for this FADOF is 90°-C.

Notice that the widest peak on the curve has a FWHM of 0.003-nm (1.2-GHz), and the total width spanned by all of the peaks is 0.035-nm (14.4-GHz).

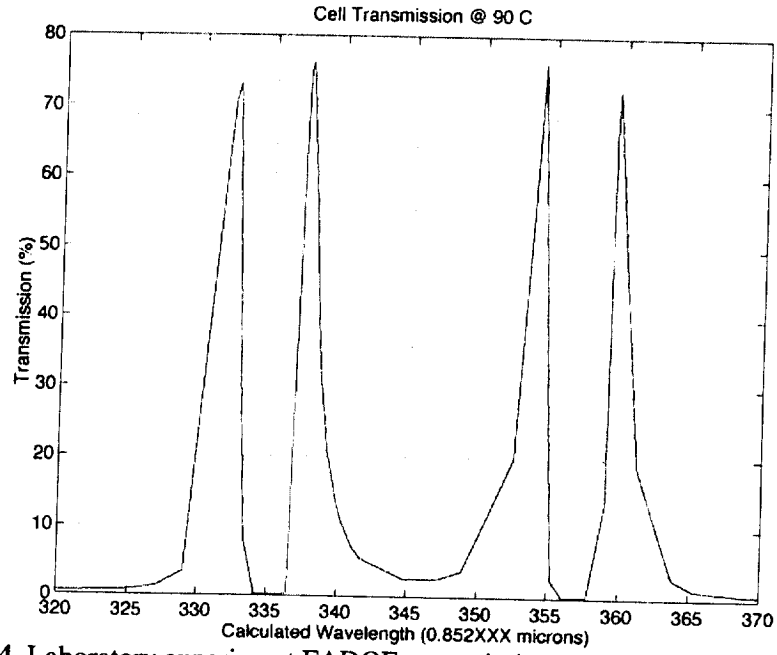

Figure 5.4 Laboratory experiment FADOF transmission curve.

5.3 System Testing Procedure and Results

A Hewlett Packard Digital Transmission Analyzer (DTA; model number 3784A) was used to test the BER of the system. The system test was done in three parts. First, the FSK uplink system was tested independently. Second, the CPK

downlink system was tested independently. Third, the output from the FSK demodulator was connected to the data input of the retro-modulator and the entire system was tested as a whole to observe any cross-modulation. All tests were repeated twice in succession on one day and again the day after. They were all performed with the transmitter clock output cabled to the receiver clock input on the DTA; no clock recovery circuits exist for the laboratory system. Table 5.2 lists the DTA settings used for all tests. A full report on the system test is available in [21].

Table 5.2 Digital transmission analyzer settings.

Parameter	Value
Data output	BINARY
TX clock rate	10-kHz*
TX clock offset	0
TX pattern	PRBS-6
TX error add	DISABLED
TX clock out	NORMAL
RX setup	AS TX
Gating type	SINGLE
Gating period	20-min*

* The independent FSK test was done at a TX rate of 20-kHz and a gating period of ten minutes.

5.3.1 Testing the Uplink

The first part of the test process was an independent uplink test. The ground receiver was not powered for this stage of the system testing. The DTA TX data out port was connected to the ground transmitter data input port with a long (100-ft) RG-59/U co-axial cable. The TX data out port was also connected to Channel 1 of the TDS-520 by using a BNC splitter and a second cable. The space receiver data output was connected to both the RX input port on the DTA and Channel 2 of the TDS-520.

After the equipment was powered up, the DTA was told to start measuring the BER of the system, and the waveforms were analyzed on the TDS-520. There were no errors in the ten-minute gating period used for this test, indicating a BER of less than 8.3×10^{-8}. The propagation delay through the uplink system was measured as 2-μs by the oscilloscope. The SNR at the input of the FSK demodulator circuit was 40-dB (Figure 3.3 on page 11 shows the operation of the demodulator), which is what the LOWCAL system equations specify for the LEO experiment.

5.3.2 Testing the Downlink

A similar setup was utilized to test the downlink system. The DTA TX output port was connected to the retro-modulator data input port with a long cable and Channel 1 of the oscilloscope with another cable. The CPK decision data output port was connected to both the DTA RX input port and Channel 2 of the TDS-520.

The DTA counted zero errors during two consecutive 20-minute gating intervals, suggesting a BER of better than 8.3×10^{-8} for the downlink. The downlink propagation delay was about 50-μs as measured by the oscilloscope.

Afterwards, Channel 2 of the TDS-520 was connected directly to the PMT output to measure the optical risetime and SNR. The optical risetime of the LCD was 80-μs, limiting the downlink to 10-kbps. The SNR out of the PMT was calculated by measuring the average and rms values of the '0' signal and the '1' signal. The SNR for a logical '0' was 11.8 V/V (21.4-dB) and the SNR for a logical '1' was 45 V/V (33.1-dB). The '0' had the greater level of optical signal power in this particular case. The SNR's are different because the PMT receiver is dominated by quantum shot noise that goes up with the optical signal power.

5.3.3 System Loop Back Test

For the final test configuration, the DTA TX output port was connected to the ground transmitter data input port, the space receiver data output was connected to the space retro-modulator input, and the ground receiver output was connected to the DTA RX input. The TX and RX signals were also connected to the TDS-520 to view the waveforms.

The system was operated at 10-kbps for 20-minutes without any detected errors. This result supports the original assumption that the uplink and downlink communication methods are completely transparent to one another.

5.4 Discussion and Conclusions

Ideally, the system tests need to be performed using a typical Shuttle experiment scenario – several five to ten minute runs with large gaps between over the course of a week. All of the experimental results agreed with theoretical calculation to within a 10% error except for the SNR at the PMT. Based upon the PMT characteristics measured by another student, the SNR should have been 50-dB, but it was only 30-dB, a difference of two orders of magnitude [16]. This is unexplained as of March 2001, but will either be explained and corrected or just compensated for by May 2001.

The system was not tested to the extent of discovering the actual BER of the various links. There are a couple of ways to rectify this, including running a BER test over a much longer gating period, or reducing the transmitted power to increase the BER to an easily detectable level. Both methods would yield results that would allow a more quantitative comparison between the theoretical and experimental results.

6. CONCLUSIONS AND SUGGESTIONS FOR FUTURE WORK

Based on the analysis herein, the LOWCAL retro-modulated optical communications system can provide a low-bandwidth link between the ground and an LEO satellite. It will operate with Zenith angles ranging from –60° to +60°. A transmitted power of 200-mW will close the link with 3.8-dB to spare, using a 6-in retro-modulator operating at 10-kbps.

Although a more repeatable demonstration is called for, the laboratory experiment verified both the LightWire concept and the possibility of full-duplex communication on a single optical beam. The only unanswered issue is the SNR discrepancy at the ground receiver.

The LOWCAL system needs more testing. An outdoor test utilizing two FADOF/PMT's is called for in the near future. It is important to test the performance of differential detection on the CPK signal. Various pieces of the experimental hardware need improvement, including the PMT decision circuit. Finally, the hardware for the Hitchhiker payload still needs perfecting (to pass NASA's shake and bake tests).

REFERENCES

1. Horan, Stephen., New Mexico State University Small Satellite Project Director, private communication. The power limit for the NMSU Small Satellite Communications System. 26 March 2001.

2. Swenson, Charles M., Steed, Clark A., DeLaRue, Imelda A., Fugate, Robert Q., "Low Power FLC-based Retro-modulator Communications System," SPIE Proceedings, 2990, pp. 296-310, in Free-Space Laser Communications Technologies IX, G. Stephen Mercherle, Ed.

3. Payne, J. A., Shay, T. M., and Garrett, C. D., "LOWCAL FSK Demodulator: Implementation, Test Procedures, and Results," Technical report # xxx.

4. Shay, T. M. and Hazzard, D. A., "Circular Polarization Keying," patent pending.

5. Dick, D. J. and Shay, T. M., "Ultra-High Noise Rejection Optical Filter," Optics Letters, 16, p. 867, June 1991.

6. Yin, B. and Shay, T. M., "Theoretical Model of Faraday Anomalous Dispersion Optical Filter," Optics Letters, 16, pp. 1617-19, October 1991.

7. Yin, B. and Shay, T. M., "Faraday Anomalous Dispersion Optical Filter in Potassium," Optics Communications, 94, pp. 30-32, November 1992.

8. Yin, B. and Shay, T. M., "Faraday Anomalous Dispersion Optical Filter for the Cs 455-nm Transition," Photonics Technology Letters, 4, 488, May 1992.

9. Chen, L., Alvarez, L. S., Wu, Y. F., Yin, B., Shay, T. M., "A Sunlight Insensitive Direct Detection Optical Communications System," Proceedings of the SPIE, 2123, pp. 448-54, 1994.

10. Shay, T. M., Payne, J. A., Horan, S., "Lightwire," patent pending.

11. Fried, D. L., "Optical Resolution through a Randomly Inhomogeneous Medium for Very Long and Short Exposures," Journal of the Optical Society of America, 56, pp. 1372-79, 1966.

12. Tracy, William, Shuttle Flight Information Officer, private communication. The typical uncertainties in the down-track position when the position vector is updated within 20 minutes of pass.

13. Hazzard, D. A., MacCannell, J. A., Lee, G., Garrett, C. D., Payne, J. A., Dahlstrom, N., and Shay, T. M., "Lightweight Optical Wavelength Communications without a Laser in Space," Proceedings of the 14th Annual AIAA/Utah State University Small Satellite Conference, 2000.

14. Wilson, K. E., Lesh, J. R., Araki, K., Arimoto, Y., "Overview of the Ground to Orbit Lasercom Demonstration," SPIE Proceedings, 2990, pp. 23-30, 1997, in Free-Space Laser Communications Technologies IX, G. Stephen Mercherle, Ed.

15. Wolfe, William L., Zissis, George J., Ed. The Infrared Handbook, Third edition, pp. 3-71.

16. MacCannell, J. A., "LOWCAL Ground Receiver: PMT Characterization Procedure and Results," Tech report # xxx.

17 Vorflusev, Valery and Kumar, Satyendra, "Phase-Separated Composite Films for Liquid Crystal Displays," Science, 283, pp. 1903-05, 19 March 1999.

18. Garrett, C. D. and Hazzard, D. A., "LOWCAL LCD Driver: Implementation, Test Procedures, and Results," Technical report # xxx.

19. Garrett, C. D., "LOWCAL Laser Driver: Implementation, Test Procedures, and Results," tech report # xxx.

20. Garrett, C. D. and Lee, G., "LOWCAL System Alignment and Calibration Procedures," Tech report # xxx.

21. Garrett, C. D., Lee, G., and MacCannell, J. A., "LOWCAL Laboratory Experiment: Test Procedures and Results," Tech report xxx.